JOURNAL OF SOLID STATE CHEMISTRY 74, 287–294 (1988)

Structure and Bonding in Lithium Ruthenate, Li_2RuO_3

A. C. W. P. JAMES* AND J. B. GOODENOUGH

Center for Materials Science and Engineering, E.T.C. 5.160, University of Texas at Austin, Austin, Texas 78712

Received November 6, 1987; in revised form December 8, 1987

The metallic lithium ruthenate Li_2RuO_3 was prepared from Li_2CO_3 and RuO_2 at high temperature; its structure was studied by powder neutron diffraction and found to be in agreement with that previously published on the basis of powder X-ray diffraction. Li_2RuO_3 has a monoclinic unit cell ($C2/c$; a = 4.9116 Å, b = 8.7586 Å, c = 9.8544 Å, β = 100.08°); its structure closely resembles that of β-Li_2SnO_3, but there is a different stacking of alternating, close-packed Li and LiM_2 (M = Ru, Sn) layers. The He-I photoelectron spectrum of Li_2RuO_3 shows an intense Fermi edge, which implies a high electronic density of states at the Fermi energy. Li_2RuO_3 is paramagnetic and obeys the Curie–Weiss law above 80 K (μ_{eff} = 1.83 μ_B, O = −167 K). A semiempirical band model for Li_2RuO_3 accounts for its metallic conductivity, photoelectron spectrum, magnetic behavior, and unusual stacking sequence. Electrochemical delithiation of Li_2RuO_3 led to a rearrangement of Ru within layers that stabilizes additional Ru–Ru bonding.

Introduction

The metallic ruthenate Li_2RuO_3 was first prepared and structurally characterized from X-ray powder diffraction data by Dulac (*1*). The diffraction pattern was indexed to a monoclinic unit cell ($C2/c$; a = 5.057 Å, b = 8.752 Å, c = 9.849 Å, β = 99.86°), and comparison of observed and calculated peak intensities led to the following structural model: a cubic close-packed oxide-ion lattice with basal planes of octahedral interstices filled alternately by Li^+ only and by $\frac{1}{3}Li^+$, $\frac{2}{3}Ru^{4+}$. The ruthenium-containing layers are further ordered to give a continuous hexagonal network of Ru^{4+} in alternate basal planes (Fig. 1). This structure is nearly identical to that of β-Li_2SnO_3 ($C2/c$; a = 5.289 Å, b = 9.022 Å, c = 10.026 Å, β = 100.35°), which has been determined by single-crystal X-ray diffraction (*2*) and by neutron powder diffraction (*3*). However, the structures of Li_2RuO_3 and β-Li_2SnO_3 differ in the stacking of LiM_2 (M = Ru, Sn) cation layers along the c axis; in both structures there are four close-packed oxide layers in the unit cell and two ordered LiM_2 layers; but in the case of β-Li_2SnO_3 the Sn^{4+} hexagonal networks in successive layers are displaced by $(0, \pm\frac{1}{6}, \frac{1}{2})$ in lattice coordinates, whereas in Li_2RuO_3 they are displaced by $(0, \frac{1}{2}, \frac{1}{2})$. It should be noted that the Dulac structure for Li_2RuO_3 described above is identical to the structure of Li_2MnO_3 given by Jansen and Hoppe (*4*) on the basis of X-ray powder diffraction data; however, the unit-cell origin is differently defined by Dulac with the result that the Ru atoms in the Dulac structure occupy 8f general positions, whereas the Jansen and

0022-4596/88 $3.00

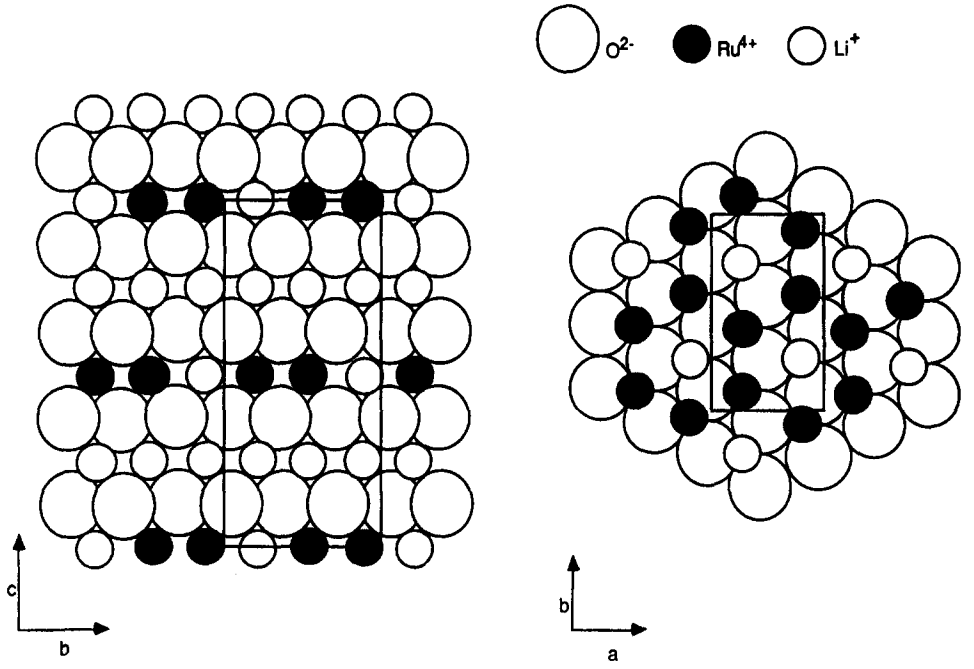

FIG. 1. Structure of Li_2RuO_3.

Hoppe structure of Li_2MnO_3 places the Mn atoms in two crystallographically inequivalent 4e sites. Projecting out the atomic positions shows that the two structures are, in fact, the same.

The purpose of this work was to confirm and refine the structural model proposed by Dulac for Li_2RuO_3 and to clarify the nature of the bonding in this material by means of He-I photoelectron spectroscopy and magnetic susceptibility measurements. Previous workers have measured the He-I PES of RuO_2 (*5, 6*) and of the pyrochlore ruthenate $Bi_2Ru_2O_7$ (*6*); they are both metallic oxides of tetravalent ruthenium and should therefore provide a useful comparison with Li_2RuO_3. Electrochemical delithiation of Li_2RuO_3 was also carried out in order to study the kinetics of lithium-ion diffusion in the all-lithium layers of the Li_2RuO_3 structure and the effect of oxidation on Ru–Ru bonding. Electrochemical delithiations of $LiCoO_2$ (*7*), $LiNiO_2$ (*8*), and $LiVO_2$ (*9*) have already been carried out. These compounds have the layered α-$NaFeO_2$ structure consisting of a cubic close-packed oxide–ion lattice with basal planes of octahedral interstices alternately filled by Li^+ and M^{3+}. In the case of $LiCoO_2$, the kinetics of the delithiation were found to be fast because of rapid Li diffusion in the all-lithium layers (*10*); extrapolating to the limit, lithium extraction gave the novel, layered ($CdCl_2$ structure) oxide CoO_2 which was stabilized by small, cooperative displacements of the Co ions (*11*). Lithium extraction from $LiNiO_2$ was also fast, although the $Ni^{4+/3+}$ couple was too strongly oxidizing for the delithiation to be carried to completion. The composition $Li_{0.5}NiO_2$ was found to transform into the novel normal spinel $Li[Ni_2]O_4$ on heating to 750 K (*8*). In the case of $LiVO_2$, the delithiated phase was stabilized by migration of vanadium ions into the lithium layers of the structure (*9*). Electrochemical delithiation of Li_2RuO_3 was un-

dertaken in the hope of finding similar interesting behavior and new synthetic pathways.

Experimental

Preparation of Li_2RuO_3. Li_2RuO_3 was prepared by the method of Dulac (*1*): RuO_2 (Ventron Alfa 99.8%) was heated in air at 1000 K for 6 hr to remove water of hydration; the resulting crystallographically pure RuO_2 was mixed with predried Li_2CO_3 (BDH AnalaR 99.5%) in stoichiometric proportion and heated at 1273 K for 24 hr in air. The resulting material was found by X-ray diffraction to be Li_2RuO_3 with about 3% of RuO_2 still present; the lithium deficiency can be accounted for by the volatility of Li_2O at 1273 K. A 4% excess of Li_2CO_3 was added and the firing was continued at 1173 K for 48 hr. The final product was crystallographically pure Li_2RuO_3 with no trace of RuO_2; it was a black powder composed of micaceous crystallites.

Diffraction measurements. X-ray diffraction measurements were performed on a Philips APD 3520 powder diffractometer. This instrument incorporates a Gaussian peak-fitting program for accurate location and measurement of diffraction peaks. Neutron powder diffraction was carried out on the instrument D1A at ILL Grenoble. Crystallographic calculations were performed on a VAX 11/780 computer with the Oxford powder crystallography suite (*12, 13*). All diffraction measurements were made at room temperature.

Photoelectron spectroscopy. The sample of Li_2RuO_3 for He-I photoelectron spectroscopy was pressed into a 13-mm-diameter pellet at 10 tons pressure and introduced into the sample-preparation chamber of an ESCALAB-5 electron spectrometer. Surface desorption of the sample was carried out overnight at up to 900 K under a dynamic vacuum $<10^{-9}$ Torr. Following transfer to the main chamber, X-ray photoelectron spectra were found to be free of signals due to carbon or other contaminants. He-I PES and HREELS spectra were obtained under a dynamic vacuum $<10^{-10}$ Torr.

Magnetic susceptibility. The magnetic susceptibility of a 14-mg sample of Li_2RuO_3 was measured between 80 and 293 K in a Cahn Instruments Faraday balance. The balance was calibrated with $CoHg(CNS)_4$ ($\chi_g = 16.44 \times 10^{-6}$ emu/g at 293 K) and the usual corrections for atomic diamagnetism were made.

Electrochemical measurements. Electrochemical extraction of lithium from Li_2RuO_3 was carried out in a test cell of the Mizushima type (*7*). Finely ground Li_2RuO_3 (about 20 mg) was pressed at 10 tons pressure onto a 1-cm-diameter grid cut from 60-mesh stainless-steel gauze. Once pressed, the grid was assembled into the cell of Fig. 2 in an argon-filled glove box. The electrolyte was 1 *M* $LiBF_4$ in purified propylene carbonate; the lithium anode and reference electrode were separated from the cathode and each other by electrolyte-soaked Whatman glass-fiber pads. The whole assembly was compressed by screwing together the stainless-steel spigots until a stable voltage was obtained between the cathode and both the counter and reference electrodes. Oxidative lithium extraction was carried out by galvanostatic charging at 10–20 μA. The experiment was interfaced to a Rade microcomputer for continuous monitoring of current and voltage.

Results

Structure of Li_2RuO_3. The structural model given by Dulac (*1*) is given in Table I; it was used as the basis for full-profile refinement of the powder neutron diffraction data for Li_2RuO_3 (Fig. 3). The lattice parameters converged rapidly to the values given. However, owing to the low neutron beam intensity at the time that the measure-

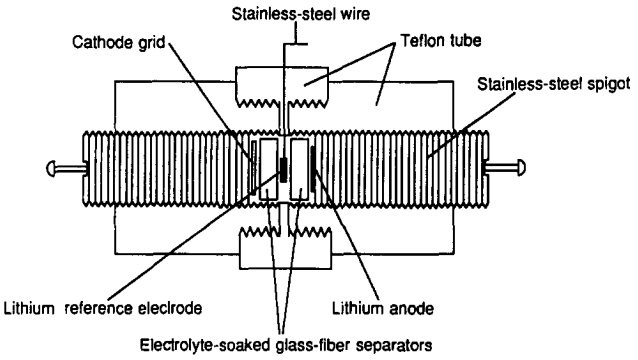

FIG. 2. Electrochemical cell used for delithiation of Li_2RuO_3.

ments were made, the data set is not of sufficient quality to enable refinement of atomic positions or temperature factors to be carried out. The profile refinement program does enable deconvolution of overlapping diffraction peaks and comparison of observed and calculated integrated peak intensities; the resulting Bragg R factor of 6% suggests that the Dulac structural model is correct, and a similar calculation definitely rules out the β-Li_2SnO_3 structure for Li_2RuO_3. The small difference in the stacking of the LiM_2 (M = Ru, Sn) layers in Li_2RuO_3 and β-Li_2SnO_3 is interesting; the β-Li_2SnO_3 structure appears to be favored on electrostatic grounds (Li_2TiO_3 also adopts this structure (*14*)), so it is probable that the interplanar Ru–Ru bonding described below accounts for the difference structure of Li_2RuO_3.

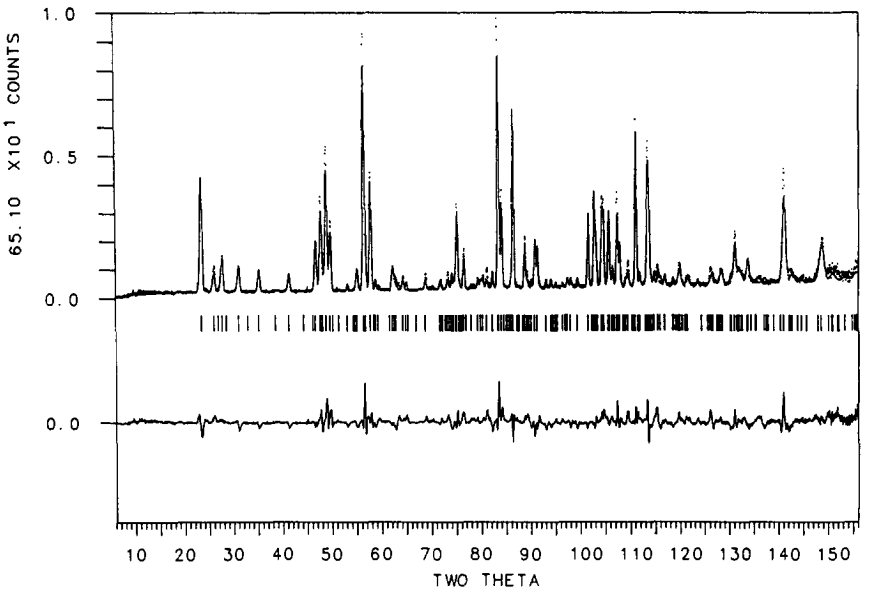

FIG. 3. Neutron diffraction pattern of Li_2RuO_3: observed (points), calculated and difference profiles (solid lines).

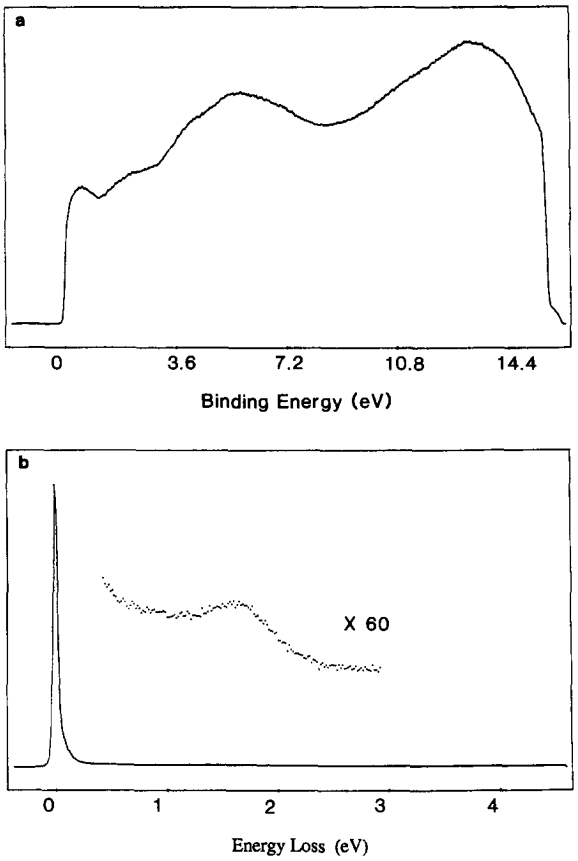

FIG. 4. (a) He-I photoelectron spectrum of Li_2RuO_3. (b) EELS spectrum of Li_2RuO_3. Incident electron energy = 25 eV.

Photoelectron spectrum. The He-I PES of Li_2RuO_3 is shown in Fig. 4. The principal feature of the spectrum is a sharp and very intense Fermi edge; this feature indicates that Li_2RuO_3 is metallic with a high electronic density of states at the Fermi level. The Fermi edge in Li_2RuO_3 is at least five times as intense relative to the adjacent oxygen 2*p* ionization signal as the Fermi edges in RuO_2 or $Bi_2Ru_2O_7$ (*5*, *6*). The HREELS spectrum of Li_2RuO_3 shows a well-defined plasmon mode centered at 1.7 eV; similar modes centered at 2.0 eV and 1.3 eV have been observed in RuO_2 and $Bi_2Ru_2O_7$, respectively.

Magnetic susceptibility. Li_2RuO_3 is paramagnetic and obeys the Curie–Weiss law at temperatures above 80 K with a relatively large, negative Weiss constant of −167 K (Fig. 5). The observed effective magnetic moment is 1.83 μ_B at 293 K, falling to 1.33 μ_B at 80 K. These results are not consistent with simple Pauli paramagnetism; they imply that there is approximately one unpaired electron spin per Ru atom in Li_2RuO_3 with strong antiferromagnetic coupling between these spins, but with no antiferromagnetic ordering down to 80 K.

Electrochemical delithiation. The open-circuit voltage (OCV) of Li_2RuO_3 against lithium is 2.6 V; this value is comparable to the 2.3–2.5 V observed for RuO_2 (*15*). Elec-

TABLE I

STRUCTURE OF Li_2RuO_3

Space group $C2/c$; a = 4.912 Å, b = 8.759 Å, c = 9.854 Å, β = 100.08°

Atom	Position	x/a	y/b	z/c	Occupancy
Ru	8f	0.249	0.083	0.001	1.00
Li(1)	4d	0.250	0.250	0.500	0.50
Li(2)	4e	0.000	0.083	0.250	0.50
Li(3)	4e	0.000	0.416	0.250	0.50
Li(4)	4e	0.000	0.750	0.250	0.50
O(1)	8f	0.124	0.249	0.118	1.00
O(2)	8f	0.124	0.584	0.118	1.00
O(3)	8f	0.124	0.916	0.118	1.00

Note. R_p = 13.5; R_{wp} = 19.1; R_b = 6.0. Number of reflections used in the refinement = 247.

$$R_p = 100 \frac{\Sigma|Y_{obs} - Y_{calc}|}{\Sigma Y_{obs}}$$

$$R_{wp} = 100 \left[\frac{\Sigma w_i |Y_{obs} - Y_{calc}|^2}{\Sigma w_i Y_{obs}^2}\right]^{1/2}$$

$$R_b = 100 \frac{\Sigma|Y_{obs} - I_{calc}|}{\Sigma I_{obs}},$$

where I = integrated Bragg intensity; Y = number of counts at angle 2θ; w = weighting factor.

trochemical delithiation of Li_2RuO_3 is kinetically fast, indicating rapid lithium-ion diffusion in the purely lithium layers of the Li_2RuO_3 structure. There is little variation in the OCV as lithium is extracted; this observation implies that lithium extraction is not topotactic, but that a distinct lithium-depleted phase is being formed. Moreover, delithiation is accompanied by structural degradation: the X-ray powder diffraction patterns of $Li_{2-x}RuO_3$ ($x > 0.2$) retain only the (002), (004), and (006) diffraction peaks of the original Li_2RuO_3 pattern; all the other peaks are very weak or undetectable, implying a high degree of disorder in the basal planes of the delithiated material. The electrochemical delithiation is not fully reversible.

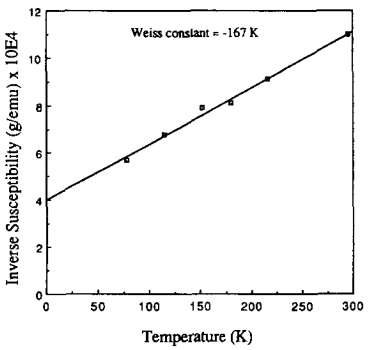

FIG. 5. Inverse magnetic susceptibility versus temperature for Li_2RuO_3.

Discussion

Figure 6 gives a schematic energy-level diagram for the Ru^{4+} 4*d*-electrons in Li_2RuO_3. The empty Ru-5*s* and filled O-2*p* bands are not indicated as the PES data and the open-circuit voltage versus lithium both show that the Fermi energy lies in the gap between these broad bands. The parent octahedral-site crystalline field splits the 4*d* manifold into empty e_σ orbitals and partially filled t_2 orbitals at the low-spin Ru^{4+} species. A trigonal component to the crystal field further splits the manifold of three t_2 orbitals into one a_1 orbital parallel to the trigonal axis and two e_π orbitals giving strong Ru–Ru overlap in the basal plane. Finally, with two Ru atoms per unit cell in the basal plane (see Fig. 1), the e_π orbitals are split into bonding and antibonding bands. Correlation splitting of the a_1 nonbonding orbitals is also indicated on the energy-level diagram. Placement of the a_1 orbital energy relative to the energies of the states of e_π parentage depends on the sign and magnitude of the trigonal component of the crystal field. From the data and calculations made on other layered compounds having cations in octahedral symmetry, we may place the singly occupied state a_1^1 above the doubly occupied bonding states of e_π parentage, but overlapped by the up-

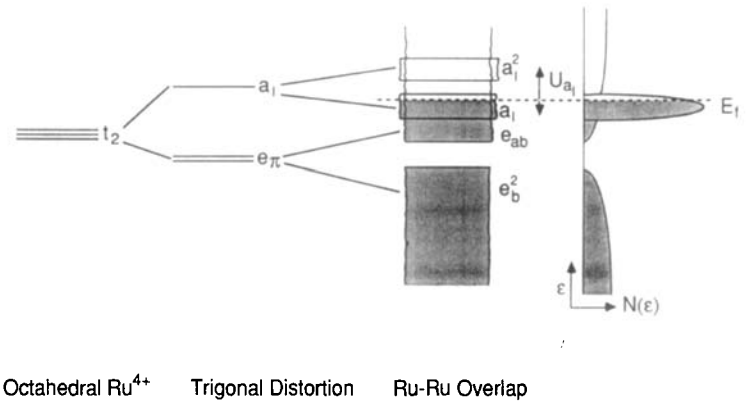

FIG. 6. Qualitative energy-level diagram for the t_2 manifold of Ru^{4+} ($4d^4$) ions in Li_2RuO_3.

per band of states of e_π parentage that is antibonding with respect to the Ru–Ru interactions. Hybridization of the a_1 orbital with the overlapping band states delocalizes the a_1 states; the situation is analogous to the hybridization between localized $4f$ and band $5d$ states that occurs in heavy-fermion systems containing rare-earth atoms (*16*).

With four $4d$-electrons per Ru^{4+} ion, the Fermi energy in such a picture would be located within the overlapping a_1^1 and antibonding bands, which is consistent with the PES observation of an anomalously high density of states at the Fermi energy. This model also accounts for the unusual magnetic behavior of Li_2RuO_3: the electrons in the partially filled a_1^1 band are essentially unpaired and give rise to the paramagnetism of Li_2RuO_3, but they are strongly coupled antiferromagnetically by the itinerant electrons in the overlapping, nearly half-filled e_π antibonding band. Similar magnetic behavior is observed in the heavy-fermion conducting compounds of the lanthanides and actinides (*16*); in these compounds the Fermi level intersects both a narrow $4f$ or $5f$ band and an overlapping broad band. The resulting "enhanced Pauli paramagnetism" shows a Curie–Weiss dependence on temperature with a large negative Weiss constant characteristic of antiferromagnetic interactions between $4f$ or $5f$ spins, but without antiferromagnetic order to low temperatures. The limiting high-temperature value of the magnetic moment is close to that predicted by crystal-field theory for the magnetically dilute $4f$- or $5f$-electron state.

Finally, partial occupancy of the a_1 orbitals allows Ru–Ru interactions perpendicular to the basal plane. Although these are weak as the Ru atoms of different layers are separated by a Li atom layer, nevertheless they appear to be strong enough to stabilize a stacking of $LiRu_2$ layers different from that of $LiSn_2$ or $LiTi_2$ layers in β-Li_2SnO_3 and Li_2TiO_3. In this connection, it is significant that Li_2MnO_3 also has the Li_2RuO_3 stacking sequence and the Mn^{4+} ion has a half-filled a_1 orbital to stabilize bonding perpendicular to the layers, whereas both Li_2IrO_3 (Ir^{4+}, $5d^5$) and Na_2PtO_3 (Pt^{4+}, $5d^6$) adopt the β-Li_2SnO_3 structure (*17, 18*). Furthermore, Li_2IrO_3 is metallic and paramagnetic with $\mu_{eff} = 1.37\ \mu_B$ at 293 K; it obeys the Curie–Weiss law with strong antiferromagnetic coupling, but no magnetic ordering down to 80 K (*18*). This magnetic behavior closely resembles that of Li_2RuO_3, suggesting that Li_2IrO_3 shares the Li_2RuO_3 bonding scheme, but with one more d-electron per

transition-metal ion so that the Fermi level intersects both the e_π antibonding band and the narrow a_1^2 band. Na_2PtO_3 is a semiconductor (*17*).

In the rutile structure of RuO_2, Ru^{4+} ions occupy octahedral sites and the Fermi energy intersects the upper half of a $d_\parallel$ band associated with Ru–Ru interactions along the *c* axis and an overlapping π^* band associated with Ru–O–Ru interactions (*5*). Therefore a work function comparable to that in Li_2RuO_3 can be expected. A comparable open-circuit voltage versus lithium for the two compounds is consistent with this expectation. More interesting is the apparent scrambling of the Ru within $LiRu_2$ layers on extraction of Li from Li_2RuO_3. Extraction of Li is accompanied by oxidation of the Ru and thus a lowering of the Fermi energy. In the case of Li_2MoO_3, formation of Mo_3 trimers within a plane has been demonstrated (*19*). Since the Ru^{4+} ion has two 4*d* holes in the t_2 manifold as compared with two electrons in a Mo^{4+} ion, a similar clustering might be expected provided electrons in a filled a_1^1 state do not destabilize the clustering configuration. Oxidation of the Ru^{4+} ions removes a_1 electrons and softens their repulsive action. We suggest that this softening is accompanied by a Ru atom rearrangement that introduces 60° Ru–Ru–Ru bond angles. The OCV and crystallographic data indicate that delithiation causes nucleation of microdomains of a second phase in which Ru atom rearrangement has taken place, but that these microdomains are too small to give coherent X-ray scattering in the basal plane. Once the Ru atoms are rearranged within a layer, the stabilization gained by the Ru–Ru bonding inhibits a reversible rearrangement on relithiation.

References

1. J.F. Dulac, *C.R. Acad. Sci. Paris Ser. B* **270,** 223 (1970).
2. G. Kreuzberg, F. Stewner, and R. Hoppe, *Z. Anorg. Allg. Chem.* **379,** 242 (1970).
3. J. L. Hodeau, M. Marezio, A. Santoro, and R. S. Roth, *J. Solid State Chem.* **45,** 170 (1982).
4. M. Jansen and R. Hoppe, *Z. Anorg. Allg. Chem.* **397,** 279 (1973).
5. N. Beatham and A. F. Orchard, *J. Electron. Spectrosc. Relat. Phenom.* **16,** 77 (1979).
6. P. A. Cox, J. B. Goodenough, P. J. Tavener, D. Telles, and R. G. Egdell, *J. Solid State Chem.* **62,** 360 (1986).
7. K. Mizushima, P. C. Jones, P. J. Wiseman, and J. B. Goodenough, *Mater. Res. Bull.* **15,** 783 (1980).
8. M. G. S. R. Thomas, W. I. F. David, J. B. Goodenough, and P. Groves, *Mater. Res. Bull.* **20,** 1137 (1985).
9. M. M. Thackeray, L. A. de Picciotto, W. I. F. David, P. G. Bruce, and J. B. Goodenough, *J. Solid State Chem.* **67,** 285 (1987).
10. M. G. S. R. Thomas, P. G. Bruce, and J. B. Goodenough, *Solid State Ionics* **18, 19,** 794 (1986).
11. M. G. S. R. Thomas, D.Phil. Thesis, Oxford, 1985.
12. K. Yvon, W. Jeitschko, and E. Parthe, *J. Appl. Crystallogr.* **10,** 73 (1977).
13. A. W. Hewat, *NBS Spec. (US)* **567,** 111–141 (1980).
14. J. F. Dorrian and R. E. Newnham, *Mater. Res. Bull.* **4,** 179 (1969).
15. D. W. Murphy, F. J. di Salvo, J. N. Carides, and J. V. Waszczak, *Mater. Res. Bull.* **13,** 1395 (1978).
16. Z. Fisk, H. R. Ott, and J. L. Smith, *J. Magn. Magn. Mater.* **47, 48,** 12 (1985).
17. V. B. Lazarev, and I. S. Shaplygin, *Russ. J. Inorg. Chem.* **23,** 803 (1978).
18. J. J. Scheer, A. E. Van Arkel, and R. D. Heyding, *Canad. J. Chem.* **33,** 683 (1955).
19. A. C. W. P. James and J. B. Goodenough, *J. Solid State Chem.*, in press.